

Quasi-Topological Insulator and Trigonal Warping in Gated Bilayer Silicene

Motohiko Ezawa

Department of Applied Physics, University of Tokyo, Hongo 7-3-1, 113-8656, Japan

Bilayer silicene has richer physical properties than bilayer graphene due to its buckled structure together with its trigonal symmetric structure. The trigonal symmetry originates in a particular way of hopping between two silicenes. It is a topologically trivial insulator since it carries a trivial \mathbb{Z}_2 topological charge. Nevertheless, its physical properties are more akin to those of a topological insulator than those of a band insulator. Indeed, a bilayer silicene nanoribbon has edge modes which are almost gapless and helical. We may call it a quasi-topological insulator. An important observation is that the band structure is controllable by applying the electric field to a bilayer silicene sheet. We investigate the energy spectrum of bilayer silicene under electric field. Just as monolayer silicene undergoes a phase transition from a topological insulator to a band insulator at a certain electric field, bilayer silicene makes a transition from a quasi-topological insulator to a band insulator beyond a certain critical field. Bilayer silicene is a metal while monolayer silicene is a semimetal at the critical field. Furthermore we find that there are several critical electric fields where the gap closes due to the trigonal warping effect in bilayer silicene.

INTRODUCTION

Silicene is a monolayer of silicon atoms forming a two-dimensional honeycomb lattice[1–3]. It has a relatively large spin-orbit (SO) gap, and its intrinsic property is the buckled structure[4–6] owing to a large ionic radius of silicon. Silicene has richer physical properties than graphene due to this property. First of all, it is a topological insulator, characterized by a full insulating gap in the bulk and helical gapless edges[6]. Furthermore, the band structure is controllable by applying the electric field E_z to a silicene sheet[7]: It has been shown that silicene undergoes a topological phase transition from a topological insulator to a band insulator as $|E_z|$ increases. It is a semimetal at the critical field E_{cr} due to its linear dispersion relation. It has many attractive and remarkable properties[8–10]. Silicene may be the most promising material now available as a topological insulator[11–14].

In this paper we analyze the band structure of bilayer silicene, which was manufactured[15] experimentally only recently. Though bilayer silicene has a trivial \mathbb{Z}_2 topological charge, we show that its physical properties are more akin to those of a topological insulator than those of a band insulator. When we switch off the Rashba SO interaction ($\lambda_R = 0$) and the interlayer SO interaction ($\lambda_{inter} = 0$), bilayer silicene shares the same edge-mode properties with a topological insulator: It has a full insulating gap in the bulk and helical gapless edges. However, helical gapless edge modes are not topologically protected because of a possible mixing between the two gapless modes present in each edge. Indeed, a small gap opens when these interactions are taken into account. Nevertheless, the physical properties are very much similar to those of a topological insulator. This is particularly so under electric field, as we shall soon see. It would be reasonable to call such a system a quasi-topological insulator.

Here we recall a recent proposal of bilayer graphene[16] with rather unphysical parameters for study of topological insulator. The model Hamiltonian is very similar to ours, and there are much in common. Nevertheless, the great merit of

our theory is that silicene is a realistic material, and any experimental test on our results is feasible. Furthermore, it is remarkable that the band structure is controllable by applying the electric field to bilayer silicene. Just as monolayer silicene undergoes a phase transition from a topological insulator to a band insulator at a certain electric field[7], bilayer silicene makes a transition from a quasi-topological insulator to a simple band insulator beyond a certain critical field. It is a metal at the critical field. There exists also a new feature. We find that the band gap closes a few times when we increase electric field, which is absent in the case of monolayer silicene. It is a trigonal warping effect.

Bilayer silicene has an additional degree of freedom how to stack two buckled monolayer silicenes. There are four types of stacking even if we concentrate on the Bernal (AB) stacking (Fig.1). For example, the forward stacking has an electron-hole symmetry but the backward stacking does not. It is possible to determine the type of stacking of a sample by experimental measurement.

This paper is organized as follows. In Section II we introduce the Hamiltonian for bilayer silicene and study the band structure of a nanoribbon. We point out by numerical calculation that the edge modes are almost gapless and helical though bilayer silicene has a trivial \mathbb{Z}_2 topological charge. In Section III we derive the effective Dirac theory to describe the low-energy physics around the K and K' points. In Section IV we investigate the band structure under homogeneous electric field based on the effective Dirac theory. Bilayer silicene is shown to become metallic at the critical electric field, though the band structure depends considerably on the type of stacking of two buckled silicenes.

SILICENE AND BILAYER SILICENE

Silicene consists of a honeycomb lattice of silicon atoms with two sublattices made of A sites and B sites. Due to the buckled structure the two sublattice planes are separated by a

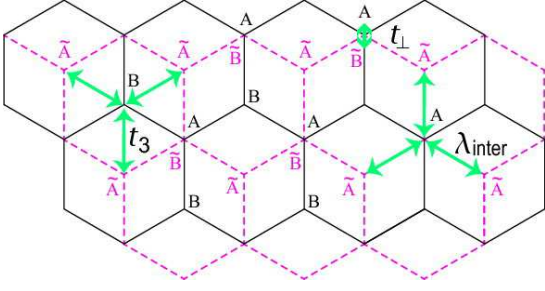


FIG. 1: (Color online) Schematic illustration of AB stacking bilayer honeycomb lattice. Bond connecting sites A, B in the top layer is indicated by solid line, while bond connecting sites \tilde{A}, \tilde{B} in the bottom layer by dashed line. The interlayer interactions are indicated by arrows together with the couplings t_{\perp} , t_3 and λ_{inter} .

distance, which we denote by 2ℓ with $\ell = 0.23\text{\AA}$. The states near the Fermi energy are π orbitals residing near the K and K' points at opposite corners of the hexagonal Brillouin zone. We refer to the K or K' point also as the K_{η} point with the valley index $\eta = \pm 1$.

The monolayer silicene system is described by the four-band second-nearest-neighbor tight binding model[17],

$$H_{\text{SL}} = -t \sum_{\langle i,j \rangle \alpha} c_{i\alpha}^{\dagger} c_{j\alpha} + i \frac{\lambda_{\text{SO}}}{3\sqrt{3}} \sum_{\langle\langle i,j \rangle\rangle \alpha\beta} \nu_{ij} c_{i\alpha}^{\dagger} \sigma_{\alpha\beta}^z c_{j\beta} - i \frac{2}{3} \lambda_{\text{R}} \sum_{\langle\langle i,j \rangle\rangle \alpha\beta} \mu_i c_{i\alpha}^{\dagger} \left(\boldsymbol{\sigma} \times \hat{\mathbf{d}}_{ij} \right)_{\alpha\beta}^z c_{j\beta}. \quad (1)$$

where $c_{i\alpha}^{\dagger}$ creates an electron with spin polarization α at site i , and $\langle i, j \rangle / \langle\langle i, j \rangle\rangle$ run over all the nearest/second-nearest neighbor hopping sites. The first term represents the usual nearest-neighbor hopping with the transfer energy $t = 1.6\text{eV}$. The second term represents the effective SO coupling with $\lambda_{\text{SO}} = 3.9\text{meV}$, where $\boldsymbol{\sigma} = (\sigma_x, \sigma_y, \sigma_z)$ is the Pauli matrix of spin, and $\nu_{ij} = +1$ if the second-nearest-neighboring hopping is anticlockwise and $\nu_{ij} = -1$ if it is clockwise with respect to the positive z axis. The third term represents the Rashba SO coupling with $\lambda_{\text{R}} = 0.7\text{meV}$, where $\mu_i = \pm 1$ for the A (B) site, and $\hat{\mathbf{d}}_{ij} = \mathbf{d}_{ij} / |\mathbf{d}_{ij}|$ with \mathbf{d}_{ij} the vector connecting two sites i and j in the same sublattice. Monolayer silicene has been shown to be a topological insulator[6, 7].

We model a bilayer silicene as two coupled buckled hexagonal lattices including inequivalent sites A, B in the top layer and \tilde{A}, \tilde{B} in the bottom layer, respectively. These are arranged according to Bernal (A - \tilde{B}) stacking, as illustrated in Fig.1. There are four types of Bernal stacking in bilayer silicene, since the top and bottom layers can be buckled upward and downward independently. Irrespective of the type, the bilayer silicene system is described by the eight-band second-nearest-neighbor tight binding model,

$$H_{\text{BL}} = H_{\text{SL}}^{\text{T}} + H_{\text{SL}}^{\text{B}} + H_{\text{inter}} \quad (2)$$

$$H_{\text{inter}} = t_{\perp} \sum_{i \in A, j \in \tilde{B}} \left(c_{i\alpha}^{\dagger} c_{j\alpha} + \text{h.c.} \right) + t_3 \sum_{i \in B, j \in \tilde{A}} \left(c_{i\alpha}^{\dagger} c_{j\alpha} + \text{h.c.} \right) + i \lambda_{\text{inter}} \sum_{i \in A, j \in \tilde{A}} c_{i\alpha}^{\dagger} \left(\boldsymbol{\sigma} \times \hat{\mathbf{d}}_{ij} \right)_{\alpha\beta}^z c_{j\beta}, \quad (3)$$

where $H_{\text{SL}}^{\text{T(B)}}$ is the Hamiltonian (1) for the top (T) or bottom (B) layer; H_{inter} is the interlayer Hamiltonian, where the first term is the nearest-neighbor interlayer vertical hopping between A sites of the top layer and \tilde{B} sites of the bottom layer with the coupling t_{\perp} , and the second term is the next-nearest-neighbor interlayer hopping between B sites of the top layer and \tilde{A} sites of the bottom layer with the coupling t_3 . There are three t_3 hopping vectors from one site, as implies the trigonal symmetry of the bilayer system. The parameters t_{\perp} and t_3 depend on the type of Bernal stacking, but we expect $t_{\perp} \gtrsim t_3 \sim 0.1t$ in all of them. The third term describes the interlayer SO interaction[18, 19] with the coupling λ_{inter} . Its magnitude would be the same order as that in graphene ($\lambda_{\text{inter}} \sim 0.5\text{meV}$).

It is readily shown that the band structure of the Hamiltonian (2) is gapped, and hence bilayer silicene is an insulator. To study what type of insulator it is, we have analyzed the energy bands of a bilayer silicene nanoribbon based on the tight-binding model (2), whose result we give in Fig.2. The band structure consists of the bulk modes and the edge modes, where the bulk modes are gapped. There exists an intriguing feature with respect to the edge modes.

When we switch off the Rashba and interlayer interactions ($\lambda_{\text{R}} = \lambda_{\text{inter}} = 0$) there emerge eight helical zero-energy modes in the edges [Fig.2(a)]. This is what we expect since the number is simply twice as much as that in monolayer silicene[6, 7]. Namely, four helical zero-energy modes arise from each monolayer silicene. Indeed, according to the bulk-boundary correspondence rule, and since the Chern number of the bilayer system is shown to be twice that of the monolayer, the number of helical edge states should also be double.

However, when we switch on these interactions ($\lambda_{\text{R}} \lambda_{\text{inter}} \neq 0$), a spin mixing occurs, as turns a two-band crossing into a two-band anticrossing and opens a small gap for the edge modes [Fig.2(b)]. This makes a sharp contrast to the monolayer case, where the gapless edge modes are protected topologically against perturbations. Despite each layer behaves as a topological insulator, an even number of such layers renders the overall system topologically trivial that is characterized by a vanishing \mathbb{Z}_2 charge. The topological triviality of a bilayer system may be understood as follows. In the bilayer system, backscattering between channels at the same edge moving in opposite directions with opposite spins is not forbidden, in contrast to the case for the monolayer system. We note that a similar behavior has been pointed out in bilayer graphene[16].

Nevertheless, the properties of bilayer silicene are more akin to those of a topological insulator than those of a band insulator. When $\lambda_{\text{R}} = \lambda_{\text{inter}} = 0$ the edge modes are purely helical, which is one of the characteristic feature of a topological insulator. When $\lambda_{\text{R}} \lambda_{\text{inter}} \neq 0$ a spin mixing occurs

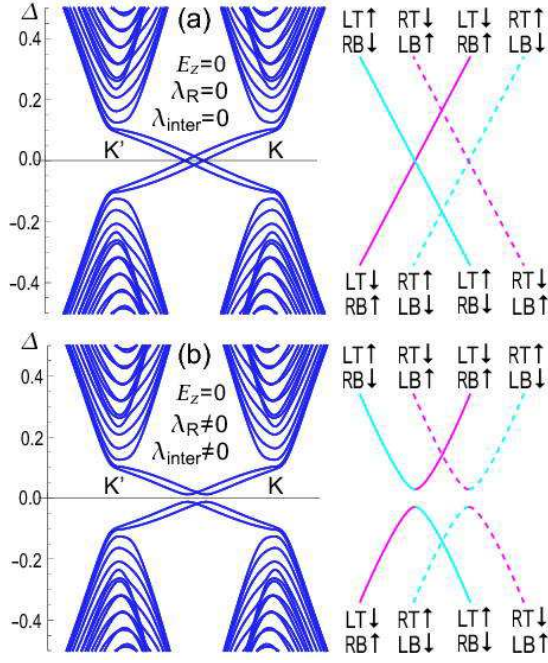


FIG. 2: (Color online) One-dimensional band structure for a bilayer silicene nanoribbon. It consists of the bulk modes and the edge modes. The vertical axis is the energy gap Δ in unit of t . The horizontal axis is k_x . (a) When the Rashba and interlayer interactions are switched off ($\lambda_R = \lambda_{\text{inter}} = 0$), there are eight bands crossing the gap, which are edge modes. There are four due to the left (L) and right (R) edges of the top (T) and bottom (B) silicenes, with each of them doubly degenerated with respect to the spin \uparrow and \downarrow . The gapless edge modes are helical. (b) When these interactions are switched on ($\lambda_R \lambda_{\text{inter}} \neq 0$), a crossing turns out to be an anticrossing due to a spin mixing, as induces a small gap. The edge modes are almost helical except for the anticrossing point. In fact, spin mixing occurs only in the vicinity of the anticrossing point. We have taken $\lambda_R/\lambda_{\text{SO}} = 1/2$ and $\lambda_{\text{inter}}/\lambda_{\text{SO}} = 1/4$ for illustration to emphasize the gap.

only around the anticrossing point, and the edge modes are almost helical away from the point, as we can confirm numerically. As we shall soon show, by applying a critical electric field, the gap becomes precisely zero at the K and K' points: Bilayer silicene becomes a metal due to a parabolic dispersion, just as monolayer silicene becomes a semimetal[7] due to a linear dispersion. It is reasonable to call such an object a quasi-topological insulator.

LOW-ENERGY DIRAC THEORY

We analyze the physics of electrons near the Fermi energy based on the low-energy effective Hamiltonian derived from the tight binding model (2). It is described by the Dirac theory around the K_η point as

$$H_\eta = \hbar v_F (k_x \tau_x^{\text{AB}} - \eta k_y \tau_y^{\text{AB}}) + H_{\text{trans}}^{\text{inter}} + H_{\text{SO}}^{\text{intra}} + H_{\text{SO}}^{\text{inter}}, \quad (4)$$

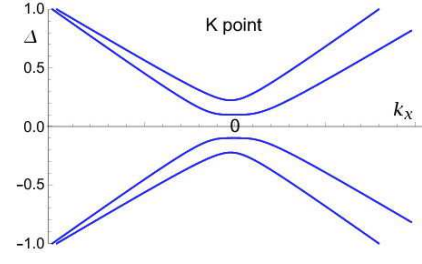


FIG. 3: (Color online) The band structure of bilayer silicene near the K point based on the Dirac Hamiltonian (4). The vertical axis is the energy gap Δ in unit of t . The horizontal axis is k_x . It is clearly gapped. There is no symmetry for $k_x \leftrightarrow -k_x$ due to the t_3 hopping term, reflecting the trigonal warping.

with

$$H_{\text{trans}}^{\text{inter}} = \frac{t_\perp}{2} (\tau_x^{\text{AB}} \tau_x^{\text{layer}} - \tau_y^{\text{AB}} \tau_y^{\text{layer}}) + \frac{t_3}{2} [k_x (\tau_x^{\text{AB}} \tau_x^{\text{layer}} + \tau_y^{\text{AB}} \tau_y^{\text{layer}})], \quad (5)$$

and

$$H_{\text{SO}}^{\text{intra}} = -\eta \tau_z^{\text{AB}} [\lambda_{\text{SO}} \sigma_z + a \lambda_R (k_y \sigma_x - k_x \sigma_y)], \quad (6)$$

and

$$H_{\text{SO}}^{\text{inter}} = \lambda_4^{\text{inter}} \tau_z^{\text{AB}} (\tau_y^{\text{layer}} \sigma_x + \eta \tau_x^{\text{layer}} \sigma_y), \quad (7)$$

where τ_a^{AB} (τ_a^{layer}) is the Pauli matrix of the sublattice (layer) pseudospin, $v_F = \frac{\sqrt{3}}{2} a t = 5.5 \times 10^5 \text{m/s}$ is the Fermi velocity, and $a = 3.86 \text{\AA}$ is the lattice constant. We show the band structure in Fig.3.

The Hamiltonian contains many parameters. Actually, λ_R and λ_{inter} are small constants with respect to the other parameters. Hence, it is a good approximation to set $\lambda_R = \lambda_{\text{inter}} = 0$ in most cases. In what follow, although we carry out numerical analysis by including the nonzero effects of λ_R and λ_{inter} , we develop an analytic formalism by assuming $\lambda_R = \lambda_{\text{inter}} = 0$. It enables us to make a simple and clear physical picture on the basis of analytic formulas. For instance, the spin $s_z = \pm 1$ becomes a good quantum number in this simplification, where the spin-chirality is given by $s = \eta s_z$. We can always check the validity of the approximation numerically.

We rewrite down the Hamiltonian H_+ explicitly in the basis $\{\psi_{A\uparrow}, \psi_{B\uparrow}, \psi_{A\downarrow}, \psi_{B\downarrow}\}^t$,

$$H_+ = \eta \begin{pmatrix} H_{11} & H_{12} \\ H_{21} & H_{22} \end{pmatrix}, \quad (8)$$

where the diagonal blocks are

$$H_{11} = \begin{pmatrix} \eta E(s, 1, 1) & \hbar v_3 k_+ \\ \hbar v_3 k_- & \eta E(s, -1, -1) \end{pmatrix}, \quad (9)$$

$$H_{22} = \begin{pmatrix} \eta E(s, 1, -1) & \eta t_\perp \\ \eta t_\perp & \eta E(s, -1, 1) \end{pmatrix}, \quad (10)$$

while the off-diagonal blocks are

$$H_{12} = H_{21} = \begin{pmatrix} 0 & \hbar v_F k_- \\ \hbar v_F k_+ & 0 \end{pmatrix}, \quad (11)$$

with $v_3 = \frac{\sqrt{3}}{2}at_3$ and $k_{\pm} = k_x \pm ik_y$. The diagonal elements are

$$E(s, t_z^{\text{AB}}, t_z^{\text{layer}}) = -t_z^{\text{AB}} s \lambda_{\text{SO}}, \quad (12)$$

where $t_z^{\text{layer}} = \pm 1$ for the upper (lower) silicene sheet. We have introduced this parameter for a later convenience, though it is irrelevant here.

We make a further simplification of the theory by reducing the 4×4 Hamiltonian to the 2×2 Hamiltonian, which is valid as the effective two-band Hamiltonian for the lower energy bands[20]. Provided $t_3 < t_{\perp}$, the reduced Hamiltonian is given by

$$H_{\text{eff}} = H_{11} - H_{12} G_{22}^0 H_{21}, \quad (13)$$

where G_{22}^0 is the 2×2 Green function,

$$G_{\alpha\alpha}^0 = (H_{\alpha\alpha} - \varepsilon)^{-1}, \quad (14)$$

with the energy ε from the Fermi level. The effective Hamiltonian around the K_{η} point reads

$$H_{\text{eff}}^{\eta} = h_B + h_w - s \lambda_{\text{SO}} \begin{pmatrix} 1 & 0 \\ 0 & -1 \end{pmatrix} - \frac{\hbar^2 v_F^2}{t_{\perp}^2} s \lambda_{\text{SO}} \begin{pmatrix} k_- k_+ & 0 \\ 0 & -k_+ k_- \end{pmatrix}, \quad (15)$$

with

$$h_B = -\frac{\hbar^2 v_F^2}{t_{\perp}} \begin{pmatrix} 0 & k_-^2 \\ k_+^2 & 0 \end{pmatrix}, \quad (16)$$

$$h_w = \eta \hbar v_3 \begin{pmatrix} 0 & k_+ \\ k_- & 0 \end{pmatrix}, \quad (17)$$

where we have used $|\varepsilon| \ll t_{\perp}$. The Hamiltonian h_B describes the quadratic Dirac Hamiltonian, which is familiar in bilayer graphene. The Hamiltonian h_w describes the trigonal warping effects. We note that the reduction into the 2×2 Hamiltonian is not available when $t_3 > t_{\perp}$.

BILAYER SILICENE IN ELECTRIC FIELD

We take a bilayer silicene sheet on the xy -plane, and apply the electric field E_z perpendicular to the plane. It generates a staggered sublattice potential $\propto \pm 2\ell E_z$ between silicon atoms at A sites and B sites in a single silicene sheet, and also a staggered sublattice potential $\propto \pm 2L E_z$ between two silicene sheets. How they enter into the Hamiltonian depends on the type of four Bernal stacking. They are

1) The top layer buckles downwardly and the bottom layer buckles downwardly (Fig.4).

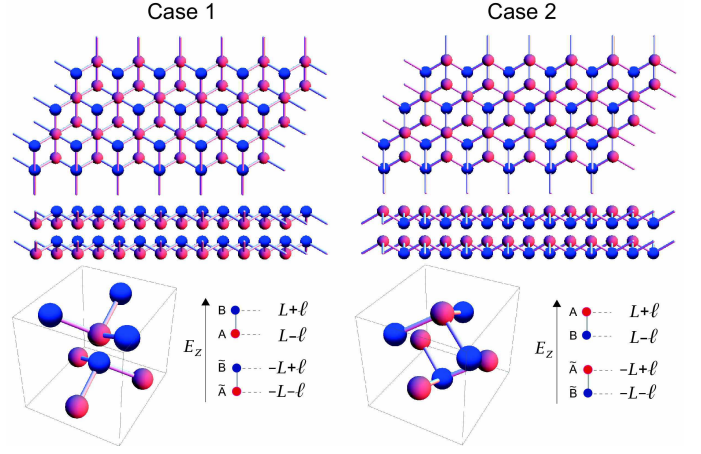


FIG. 4: (Color online) Illustration of the forward Bernal (AB) stacking bilayer silicene. The order of sites is B, A, \bar{B}, \bar{A} for the case 1 and A, B, \bar{A}, \bar{B} for the case 2 from the top to the bottom.

2) The top layer buckles upwardly and the bottom layer buckles upwardly (Fig.4).

3) The top layer buckles upwardly and the bottom layer buckles downwardly (Fig.5).

4) The top layer buckles downwardly and the bottom layer buckles upwardly (Fig.5).

Here, upward (downward) means that A site is higher (lower) than B on the same layer.

Silicon atoms prefer having the neighboring atoms in regular tetrahedron directions, and hence the case 1 seems most likely. The cases 3 and 4 are identical by reversing the whole system, and the energy spectrum is identical between them. Thus it is enough to investigate the cases 1, 2 and 3. These three systems can not be transformed only by the translation. It is necessary to rotate 120 degrees after translation. We call the case 1 and 2 (3 and 4) as the forward (backward) Bernal stacking. The forward (backward) Bernal stacking bilayer silicene is shown in Fig.4 (5), where the order of sites is A, B, \bar{A}, \bar{B} (B, A, \bar{A}, \bar{B}). The electric energy depends on the order. The magnitude of the interlayer SO interaction λ_{inter} depends on the stacking type.

The effective Hamiltonian for the forward stacking is given by

$$H = H_{\text{BL}} + (L\tau_z^{\text{layer}} + \ell\tau_z^{\text{AB}}) \sum_{i\alpha} \eta_i E_z^i c_{i\alpha}^\dagger c_{i\alpha}, \quad (18)$$

while the one for the backward stacking is given by

$$H = H_{\text{BL}} + (L - \ell\tau_z^{\text{AB}})\tau_z^{\text{layer}} \sum_{i\alpha} \eta_i E_z^i c_{i\alpha}^\dagger c_{i\alpha}, \quad (19)$$

where H_{BL} is given by (2). Accordingly, the Dirac Hamiltonian (4) is modified as

$$H_{\eta} = H_{\eta}^0 + E(s, t_z^{\text{AB}}, t_z^{\text{layer}}), \quad (20)$$

where H_{η}^0 is the Dirac Hamiltonian (4), and

$$E(s, t_z^{\text{AB}}, t_z^{\text{layer}}) = -s \lambda_{\text{SO}} t_z^{\text{AB}} + (L\tau_z^{\text{layer}} + \ell\tau_z^{\text{AB}}) E_z \quad (21)$$

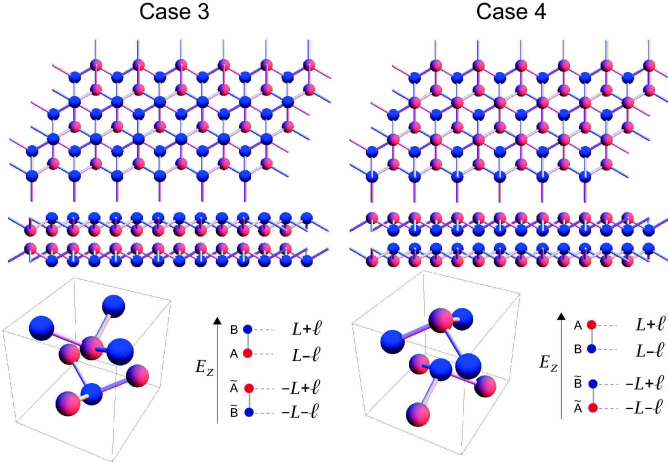


FIG. 5: (Color online) Illustration of the backward Bernal (AB) stacking bilayer silicene. The order of sites is $B, A, \tilde{A}, \tilde{B}$ for the case 3 and $A, B, \tilde{B}, \tilde{A}$ for the case 4 from the top to the bottom.

for the forward stacking, and

$$E(s, t_z^{\text{AB}}, t_z^{\text{layer}}) = -s\lambda_{\text{SO}}t_z^{\text{AB}} + \tau_z^{\text{layer}}(L - \ell\tau_z^{\text{AB}})E_z \quad (22)$$

for the backward stacking. The modification is very simple for the four-band theory: The electric field is incorporated into the Dirac Hamiltonian (8) only by changing the diagonal elements $E(s, t_z^{\text{AB}}, t_z^{\text{layer}})$ in (9) and (10) with (21) or (22).

We first investigate the case 1, and then the cases 3 and 4. The case 2 is investigated at the end since the two-band Hamiltonian is unavailable.

Forward Bernal Stacking in Electric Field: Case 1, $BA-\tilde{B}\tilde{A}$ type

In the case 1 of the forward Bernal stacking, the effective two-band Hamiltonian under homogeneous electric field is derived as

$$H_{\text{eff}}^{\eta} = h_B + h_w + m_D \begin{pmatrix} 1 & 0 \\ 0 & -1 \end{pmatrix} - \frac{\hbar^2 v_F^2}{t_{\perp}^2} \{ (L + \ell) E_z + s\lambda_{\text{SO}} \} \begin{pmatrix} k_- k_+ & 0 \\ 0 & -k_+ k_- \end{pmatrix}, \quad (23)$$

with the Dirac mass

$$m_D = (L - \ell) E_z - s\lambda_{\text{SO}}. \quad (24)$$

The energy spectrum has the electron-hole symmetry. The spectrum becomes gapless when $m_D = 0$, or $E_z = E_{\text{cr}0}$ with

$$E_{\text{cr}0} = \frac{s\lambda_{\text{SO}}}{L - \ell}, \quad (25)$$

which occurs at $k_{\pm} = 0$. We can show that the band gap is given as

$$\Delta = 2|m_D|, \quad (26)$$

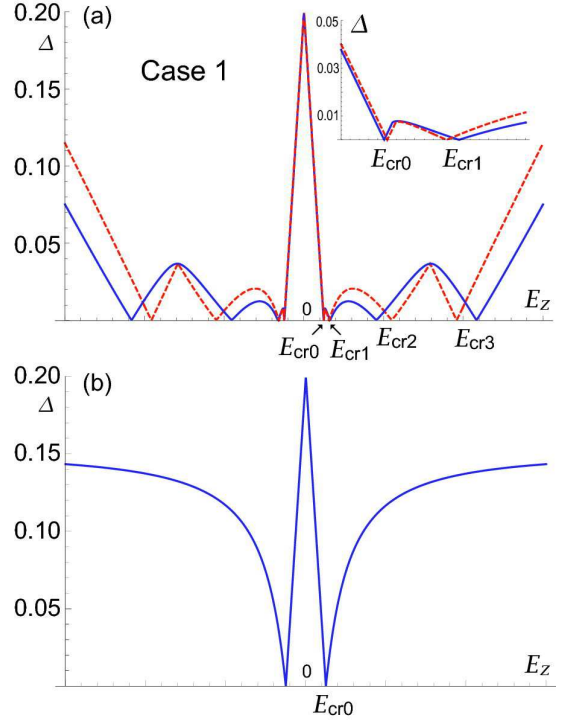


FIG. 6: (Color online) (a) Band gap Δ of the forward stacking silicene as a function of the electric field E_z for the case 1. The gap closes at the critical points $E_{\text{cr}0}, E_{\text{cr}1}, E_{\text{cr}2}, E_{\text{cr}3}$. Bilayer silicene is an insulator except for these points. We note that the critical points $E_{\text{cr}2}$ and $E_{\text{cr}3}$ are missed in the effective two-band theory. (b) The band gap in the limit $t_3 \rightarrow 0$, where all the critical points collapse to one. Solid (dashed) curve is the band gap obtained based on the Dirac Hamiltonian (20) by taking $\lambda_R/\lambda_{\text{SO}} = 1/2$, $\lambda_{\text{inter}}/\lambda_{\text{SO}} = 1/4$ and $\lambda_{\text{SO}}/t = 1/10$ for illustration to emphasize the effects ($\lambda = \lambda_{\text{inter}} = 0$ for comparison). They show qualitatively the same behavior.

for $|E| < E_{\text{cr}0}$. See also Fig.6 which we have derived by numerical calculations, where we compare the two results with $\lambda_R\lambda_{\text{inter}} \neq 0$ and with $\lambda_R = \lambda_{\text{inter}} = 0$. We show the band structure at the critical electric field in Fig.7.(a). The band structure at the Fermi energy is parabolic, which is reminiscent of bilayer graphene. We conclude that the system is a quasi-topological (band) insulator when the Dirac mass is negative (positive).

The gap closes at $E_z = \pm E_{\text{cr}0}$, where it is a metal due to gapless modes exhibiting a parabolic dispersion relation: See the band structure at $E_z = E_{\text{cr}0}$ in Fig.7(a). It follows that up-spin ($s_z = +1$) electrons are gapless at the K point ($\eta = +1$), while down-spin ($s_z = -1$) electrons are gapless at the K' point ($\eta = -1$). Namely, spins are perfectly up (down) polarized at the K (K') point under the uniform electric field $E_z = E_{\text{cr}0}$. Recall that monolayer silicene is a semimetal due to a linear dispersion at the critical point[7].

There exists one more critical point implied by the 2×2 Hamiltonian, where the spectrum become gapless. The condition is that the Hamiltonian (23) itself becomes zero, as im-

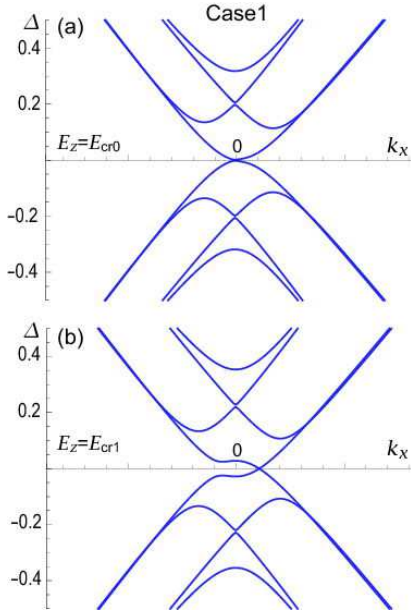


FIG. 7: (Color online) Band structure of the forward Bernal (AB) stacking bilayer silicene (a) at the critical field E_{cr0} and (b) at the critical field E_{cr1} for the case 1. The horizontal axis is k_x . (a) The gapless mode is parabolic, showing that it is a metal at $E = E_{cr0}$. (b) At $E = E_{cr1}$, there is no symmetry for $k_x \leftrightarrow -k_x$ due to the t_3 hopping term, reflecting the trigonal warping. A 3-dimensional figure is given in Fig.8.

plies

$$(L - \ell)E_z - s\lambda_{SO} - \frac{\hbar^2 v_F^2}{t_\perp^2} \{(L + \ell)E_z + s\lambda_{SO}\} k_- k_+ = 0, \quad (27)$$

$$\hbar v_3 k_+ - \frac{\hbar^2 v_F^2}{t_\perp} k_-^2 = 0. \quad (28)$$

There are two solutions with $k_y = 0$. The first one is $k_x = 0$, where E_z is given by (25). The new solution is given by solving

$$k_x = \pm \frac{t_\perp \sqrt{-(L - \ell)E_z + s\lambda_{SO}}}{\hbar v_F \sqrt{-(L + \ell)E_z - s\lambda_{SO}}} = \frac{v_3 t_\perp}{\hbar v_F^2}, \quad (29)$$

which yields

$$E_{cr1} = \frac{(1 + v_3^2/v_F^2)s\lambda_{SO}}{(L - \ell) - v_3^2/v_F^2(L + \ell)}, \quad (30)$$

as illustrated in Fig.7(b). There are two more solutions by performing $\pm 2\pi/3$ rotations in the (k_x, k_y) plane around $(0, 0)$ with the same critical field E_{cr1} due to the trigonal symmetry, as illustrated in Fig.8.

Actually there is two more critical point, E_{cr2} and E_{cr3} , which are present in the original Hamiltonian (8) with (21) but missed in the reduced two-band model (23), as we demonstrate in Fig.6(a). Note that $E_{cri} \rightarrow E_{cr0}$ for $i = 1, 2, 3$ as $t_3 \rightarrow 0$. Namely, these three critical points are generated by the t_3 hopping effect.

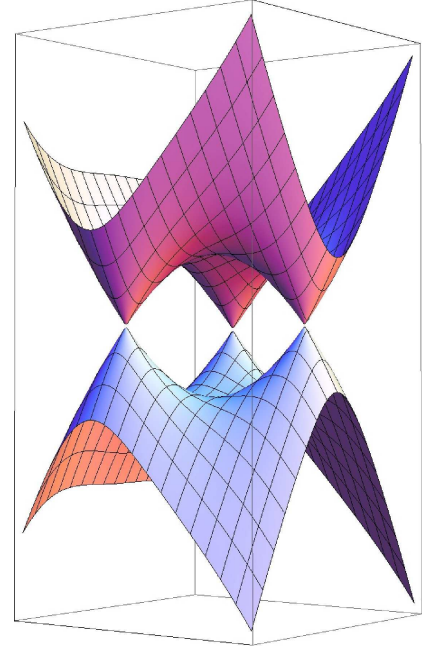


FIG. 8: (Color online) Band structure of the forward Bernal (AB) stacking bilayer silicene at the critical field E_{cr1} for the case 1. The Dirac cone is split into three cones, where the band touches the Fermi level. We have taken $\lambda_R/\lambda_{SO} = 1/2$, $\lambda_{inter}/\lambda_{SO} = 1/4$ and $\lambda_{SO}/t = 1/10$ for illustration.

Backward Bernal Stacking in Electric Field: Cases 3 and 4, $BA-\tilde{A}\tilde{B}$ and $AB-\tilde{B}\tilde{A}$ types

The cases 3 and 4 are identical by reversing the whole system. In the case of the backward Bernal stacking, the effective two-band Hamiltonian under homogeneous electric field is derived as

$$H_{\text{eff}}^\eta = h_B + h_w + m_D \begin{pmatrix} 1 & 0 \\ 0 & -1 \end{pmatrix} - \ell E_z \begin{pmatrix} 1 & 0 \\ 0 & 1 \end{pmatrix} - \frac{\hbar^2 v_F^2}{t_\perp^2} (L E_z + s\lambda_{SO}) \begin{pmatrix} k_- k_+ & 0 \\ 0 & -k_+ k_- \end{pmatrix} + \frac{\hbar^2 v_F^2}{t_\perp^2} \ell E_z \begin{pmatrix} k_- k_+ & 0 \\ 0 & k_+ k_- \end{pmatrix}, \quad (31)$$

with the Dirac mass

$$m_D = L E_z - s\lambda_{SO}. \quad (32)$$

The energy spectrum has no electron-hole symmetry. The Fermi energy is moved to $-\ell E_z$ by the presence of the electric field. The spectrum becomes gapless at $E_z = E_{cr0}$ with

$$E_{cr0} = \frac{s\lambda_{SO}}{L}, \quad (33)$$

which occurs at $k_\pm = 0$. We can show that the band gap is given as

$$\Delta = 2\lambda_{SO} - 2L|E_z|, \quad (34)$$

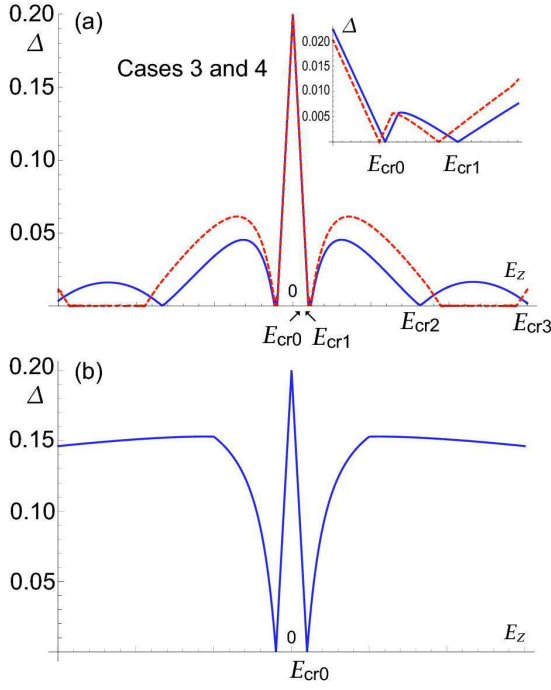


FIG. 9: (Color online) (a) The band gap Δ of the backward stacking silicene as a function of the electric field E_z for the cases 3 and 4. The gap closes at the critical points E_{cr0} , E_{cr1} , E_{cr2} and E_{cr3} . Bilayer silicene is an insulator except for these points. We note that the critical points E_{cr2} and E_{cr3} are missed in the effective two-band theory. (b) The band gap in the limit $t_3 \rightarrow 0$, where all the critical points collapse to one. Solid (dashed) curve is the band gap obtained based on the Dirac Hamiltonian (20) by taking $\lambda_R/\lambda_{SO} = 1/2$, $\lambda_{inter}/\lambda_{SO} = 1/4$ and $\lambda_{SO}/t = 1/10$ for illustration to emphasize the effects ($\lambda = \lambda_{inter} = 0$ for comparison). The band gap is identical for the cases 3 and 4.

for $|E| < E_{cr0}$. See also Fig.9 we derive by numerical calculations.. We note that the energy spectrum is identical between the cases 3 and 4. We show the band structure at the critical electric field in Fig.10(a). The band structure at the Fermi energy is parabolic, which is reminiscent of bilayer graphene.

There exists one more critical field implied by the 2×2 Hamiltonian, where the spectrum becomes gapless. The condition is that the Hamiltonian (23) itself becomes zero, as implies

$$LE_z - s\lambda_{SO} - \frac{\hbar^2 v_F^2}{t_{\perp}^2} (LE_z + s\lambda_{SO}) k_- k_+ = 0, \quad (35)$$

$$\hbar v_3 k_+ - \frac{\hbar^2 v_F^2}{t_{\perp}} k_-^2 = 0. \quad (36)$$

There are two solutions with $k_y = 0$. The first one is $k_x = 0$, where E_z is given by (33). The new solution is given by solving

$$k_x = \pm \frac{t_{\perp} \sqrt{LE_z - s\lambda_{SO}}}{\hbar v_F \sqrt{LE_z + s\lambda_{SO}}} = \frac{v_3 t_{\perp}}{\hbar v_F^2}, \quad (37)$$

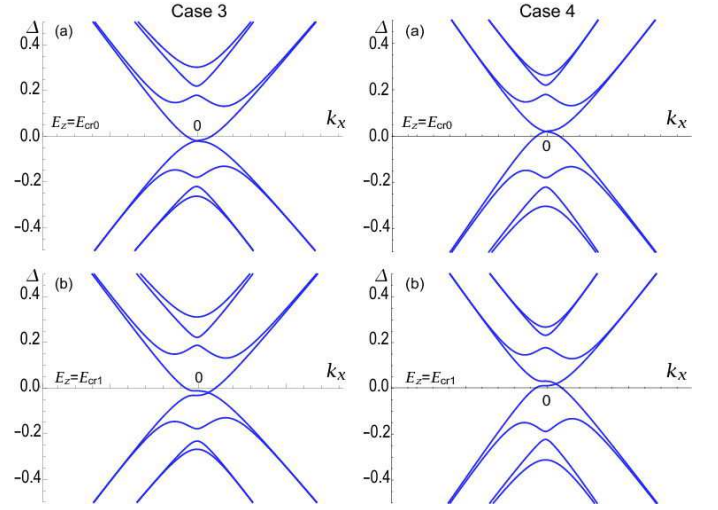


FIG. 10: (Color online) Band structure of the backward Bernal (AB) stacking bilayer silicene at the critical fields E_{cr0} and E_{cr1} for the cases (3) and (4). The gap structure Δ for the case 4 is given by $-\Delta$ for the case 3. The gap closes at $k_x = 0$ for E_{cr0} , but at $k_x \neq 0$ for E_{cr1} due to the trigonal warping. The Fermi level is the one at $E_z = 0$.

which yields

$$E_{cr1} = \frac{(1 + v_3^2/v_F^2)s\lambda_{SO}}{(1 - v_3^2/v_F^2)L}. \quad (38)$$

There are two more solutions by performing $\pm 2\pi/3$ rotations in the (k_x, k_y) plane around $(0, 0)$ with the same critical field E_{cr1} due to the trigonal symmetry.

Actually there are two more critical points, E_{cr2} and E_{cr3} , which are present in the original Hamiltonian (8) with (22) but missed in the reduced two-band model (31), as we demonstrate in Fig.9. It is intriguing that the band is flat for $E_z > E_{cr2}$. Note that $E_{cr1} \rightarrow E_{cr0}$ but $E_{cr2} \rightarrow \infty$ as $t_3 \rightarrow 0$. Namely, these two critical points are generated by the t_3 hopping effect.

Forward Bernal Stacking in Electric Field: Case 2, $AB-\tilde{A}\tilde{B}$ type

Finally we investigate the case 2. In this case, since we have $t_3 > t_{\perp}$, the two-band Hamiltonian of the type (13) is unavailable. We are unable to present analytic formulas. We have calculated the band gap numerically, which we show in Fig.11. The number of the critical electric field is found to be reduced to two.

DISCUSSIONS

Bilayer silicene has such a peculiar feature that its physical properties are more akin to those of a topological insulator than those of a band insulator though it has a trivial \mathbb{Z}_2 topological charge. Namely it is characterized by a full insulating

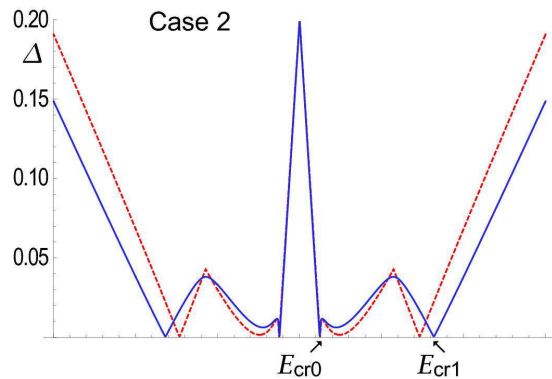


FIG. 11: (Color online) (a) The band gap Δ of the forward stacking bilayer silicene as a function of the electric field E_z for the case 2. The gap closes at the critical points E_{cr0} and E_{cr1} . Bilayer silicene is an insulator except for these points.

gap in the bulk and almost helical gapless edges. It exhibits a similar behavior as monolayer silicene under electric field E_z . Physical properties are very similar to those of a topological insulator for $|E_z| < E_{cr0}$, while they become those of a band insulator for $|E_z| > E_{cr0}$ with a transition point E_{cr0} . The gap closes precisely at the transition point, where bilayer silicene is a metal while monolayer silicene is a semimetal.

As we have discussed in the case of monolayer silicene[7], therefore, by applying an inhomogeneous electric field, we would be able to create metallic regions anywhere within a bilayer silicene sheet where helical zero-energy modes are confined. Furthermore, by rolling up a sheet, we may consider a double-wall silicon-nanotube, and by applying an electric field perpendicular to the tube axis, we would be able to create metallic channels parallel to the tube axis where spin currents are conveyed[10].

I am very much grateful to N. Nagaosa for many fruitful

discussions on the subject. This work was supported in part by Grants-in-Aid for Scientific Research from the Ministry of Education, Science, Sports and Culture No. 22740196.

-
- [1] P. Vogt, P. De Padova, C. Quaresima, J. A., E. Frantzeskakis, M. C. Asensio, A. Resta, B. Ealet and G. L. Lay; *Phys. Rev. Lett.* **108** (2012) 155501.
 - [2] C.-L. Lin, R. Arafune, K. Kawahara, N. Tsukahara, E. Minamitani, Y. Kim, N. Takagi, M. Kawai; *Appl. Phys. Express* **5** (2012) 045802.
 - [3] A. Fleurence, R. Friedlein, T. Ozaki, H. Kawai, Y. Wang and Y. Yamada-Takamura; *Phys. Rev. Lett.* **108** (2012) 245501.
 - [4] K. Takeda and K. Shiraishi; *Phys. Rev. B* **50** (1994) 075131.
 - [5] S. Cahangirov, M. Topsakal, E. Aktürk, H. Sahin and S. Ciraci; *Phys. Rev. Lett.* **102** (2009) 236804.
 - [6] C.-C. Liu, W. Feng and Y. Yao; *Phys. Rev. Lett.* **107** (2011), 076802.
 - [7] M. Ezawa; *New J. Phys.* **14** (2012) 033003.
 - [8] M. Ezawa; *J. Phys. Soc. Jpn.* **81** (2012) 064705.
 - [9] M. Ezawa; *Phys. Rev. Lett.* **109** (2012) 055502.
 - [10] M. Ezawa; *Europhysics Letters* **98** (2012) 67001.
 - [11] M.Z Hasan and C. Kane; *Rev. Mod. Phys.* **82** (2010) 3045.
 - [12] X.-L. Qi and S.-C. Zhang; *Rev. Mod. Phys.* **83** (2011) 1057.
 - [13] C. L. Kane and E. J. Mele; *Phys. Rev. Lett.* **95** (2005) 226801.
 - [14] C. Wu, B.A. Bernevig and S.-C. Zhang; *Phys. Rev. Lett.* **96** (2006) 106401.
 - [15] B. Feng, Z. Ding, S. Meng, Y. Yao, X. He, P. Cheng, L. Chen and K. Wu; *Nano Lett.* **12** (2012) 3507.
 - [16] E. Prada, P. San-Jose, L. Brey and H.A. Fertig; *Solid State Communications* **151** (2011) 1075.
 - [17] C.-C. Liu, H. Jiang and Y. Yao; *Phys. Rev. B* **84** (2011) 195430.
 - [18] G. Dresselhaus and M. S. Dresselhaus; *Phys. Rev. A* **140** (1965) 401.
 - [19] F. Guinea; *New Journal of Physics* **12** (2010) 083063.
 - [20] E. McCann and V. I. Fal'ko; *Phys. Rev. Lett.* **96** (2006) 086805.